This is the pre-peer reviewed version of the article: Mohanty J R, Parhi D R K, Ray P K, Verma B B, Prediction of residual life under interspersed mixed mode (I and II) overloads by Artificial Neural Network, *Fatigue Fract Engng Mater Struct* **32**(2009), 1020-1031, which has been published in the final form at http://www3.interscience.wiley.com/cgi-bin/fulltext/122664610/HTMLSTART

Prediction of residual fatigue life under interspersed mixed mode (I and II) overloads by Artificial Neural Network

J. R. Mohanty[a], B. B. Verma[a], D. R. K Parhi[b], P. K. Ray[b*]

[a] *Department of Metallurgical and Materials Engineering*

[b] *Department of Mechanical Engineering*

National Institute of Technology, Rourkela 769008, India

Abstract

Mixed mode (I and II) overloads are often encountered in an engineering structure due to either alteration of the loading direction or the presence of randomly oriented defects. Prediction of fatigue life in these cases is more complex than that of mode-I overloads. The objective of this study is to explore the use of an artificial neural network (ANN) model for the prediction of fatigue crack growth rate under interspersed mixed mode (I and II) overload. The crack growth rates as predicted by the ANN method on two aluminum alloys, 7020 T7 and 2024 T3, have been compared with the experimental data and an Exponential Model. It is observed that the predicted results are in good agreement and facilitate determination of residual fatigue life.

Keywords: Exponential model; Mode-mixity; Retardation parameters, Multi-layer perceptron, Normalized mean square error.

***** Corresponding author. Tel.: +91 661 2462518 (P. K. Ray)
Email addresses: pkray@nitrkl.ac.in, prabal_kray@yahoo.com

Nomenclature

a	crack length measured from edge of the specimen (mm)
a_{i}	crack length corresponding to the 'i^{th}' (initial) step (mm)
a_{j}	crack length corresponding to the 'j^{th}' step (mm)
a_{d}	retarded crack length (mm)
$a_{\mathrm{d}}^{\mathrm{A}}$	retarded (ANN) crack length (mm)
$a_{\mathrm{d}}^{\mathrm{EN}}$	retarded (exponential) crack length (mm)
$a_{\mathrm{d}}^{\mathrm{EX}}$	retarded (experimental) crack length (mm)
A', B', C', D'	curve fitting constants in the Exponential Model
'cgr'	crack growth rate
da/dN	crack growth rate (mm/cycle)
E	modulus of elasticity (MPa)
E_{rr}	sum-squared error
f(.)	activation function
K	stress intensity factor ($\mathrm{MPa}\sqrt{\mathrm{m}}$)
K_{I}	mode-I stress intensity factor ($\mathrm{MPa}\sqrt{\mathrm{m}}$)
K_{II}	mode-II stress intensity factor ($\mathrm{MPa}\sqrt{\mathrm{m}}$)
K_{C}	plane stress fracture toughness ($\mathrm{MPa}\sqrt{\mathrm{m}}$)
ΔK	stress intensity factor range ($\mathrm{MPa}\sqrt{\mathrm{m}}$)
$\dfrac{K_{\mathrm{II}}}{K_{\mathrm{I}}+K_{\mathrm{II}}}$	mode-mixity
l	dimensionless factor in the 'Exponential Model' formulation
'lay'	layer number
m	specific growth rate
'MM'	mode-mixity
'msif'	maximum stress intensity factor
m_{ij}	specific growth rate in the interval i-j
N	number of cycles or fatigue life
N_{i}	number of cycles corresponding to the 'i^{th}' step

N_j	number of cycles corresponding to the 'j^{th}' step
N_f	final number of cycles
N_d	number of delay cycle
N_d^A	number of delay cycle (ANN)
N_d^{EN}	number of delay cycle (exponential)
N_d^{EX}	number of delay cycle (experimental)
N_f^A	final number of cycles (ANN)
N_f^{EN}	final number of cycles (exponential)
N_f^{EX}	final number of cycles (experimental)
r	label for r^{th} neuron in hidden layer 'lay-1'
S	label for s^{th} neuron in the hidden layer 'lay'
'sifr'	stress intensity factor range
t	iteration number
w	plate width (mm)
$W_{sr}^{\{lay\}}$	weight of the connection from neuron r in layer 'lay-1' to neuron 's' in layer 'lay'
y_1, y_2, y_3	inputs to the ANN
$X_1..X_4$, $Y_1..Y_4$ and $Z_1..Z_4$	curve fitting constants in the 'Exponential Model'
ν	Poison's ratio
α	momentum coefficient
α_1	ratio of mode-I and mode-II plane stress fracture toughness
β	loading angle
θ_{actual}	neural network output
$\theta_{desired}$	desired output
η	learning rate
$\delta_s^{\{lay\}}$	local error gradient
σ_{ys}	yield point stress (MPa)

1. Introduction

During service, structures and components are generally subjected to cyclic loading, where the mode of loading may vary from pure mode-I, II and III to mixed-mode. Under these situations, load amplitudes may change either occasionally or permanently (for a particular period) leading to mixed mode (I and II) overload or mixed mode block loading. Similar to single mode-I overload, mixed mode (I and II) spike overload also retards the crack growth rate and consequently affects the fatigue life. The observed retardation effect decreases with an increasing amount of mode-II component of the overload [1, 2].

The problem of mixed mode (I and II) fatigue has been extensively investigated since the pioneer contribution of Iida and Kobayashi [3]. Several investigators [4-8] have proposed various models of mixed mode (I and II) fatigue crack growth. A few research works [1, 2, 9] have been done to analyze the mixed mode (I and II) overload fatigue. However, from life prediction point of view, no model is available, to the knowledge of the authors, so far as mixed-mode overloads are concerned. Earlier a preliminary attempt has been taken by the authors [10] to evaluate various retardation parameters under mixed mode (I and II) spike overload using an Exponential Model. Later some improvements [11] have been suggested to extend it to predict the end of life under these situations.

In recent years, artificial neural network (ANN) approach has emerged as a new branch of soft-computing used in various fields of science including fatigue. It is an information processing system which learns by examples without requiring the theory behind a phenomenon. It is successfully used where the relationships of inputs and outputs are non-linear. A brief literature survey regarding the use of ANN in the field of fatigue has been done by Jia and Davalos [12] in their research paper. They used ANN to predict fatigue crack growth rate that would facilitate the development of design guidelines for hybrid material bonded interfaces. Although, artificial neural network finds its application in the field of fatigue, but automatic prediction of fatigue life under interspersed mixed mode (I and II) overload by using the above method is lacking. In the present work ANN has been used to evaluate various mixed mode (I and II) overload induced retardation parameters as well as residual fatigue life from predicted da/dN–ΔK

curve of post-overload period. The results have been compared with those obtained from the extended exponential model earlier proposed by the [11]. It has been observed that the predicted ANN results are in good agreement with the experimental data as well as the above model results.

2. Artificial Neural Network

2.1 A brief introduction to the approach

Human brain is made up of hundreds of millions brain neurons densely interconnected by synapses. Dendrites receive information and activate cells to transfer information to the other neurons by axons. ANNs are computational models similar to human brain intelligence system, which simulate the function of biological neural network composed of neurons. Each neuron receives different input signals which in turn sums all the input signals (with suitable weights) and, if this sum is greater than a chosen threshold, it produces one output signal.

More precisely, the system is composed of a layer of input neurons, a layer of output neurons and one or more layers of hidden neurons. Neurons in each layer are interconnected to subsequent layer neurons with each interconnection having associated connection strength (or weight). Various non-linear activation functions, such as sigmoidal, tanh or radial (Gaussian), are used to model the neuron activity. There are three types of training, the supervised, unsupervised and reinforcement. The input-output sets are divided into two groups in case of supervised training. The first group is used for the training phase and the second group for the validation phase. The network is trained by optimizing corresponding weights in such a way that the significant outputs can be obtained for the inputs not belonging to the training set. The unsupervised training is based on organizing the structure so that similar stimuli activate similar neurons where there is no pre-defined output and the network finds differences and affinities between the inputs. In reinforcement learning, one form of supervised training attempts to learn input-output vectors by trial and error through maximizing a performance function (named reinforcement signal).

Some ANNs are classified as feed forward while others are recurrent depending on how data are processed through the network. Among the various classifications,

depending on the structure and training phase, multi-layer perceptron (MLP) is the most popular and widespread ANN architecture for engineering problems. They are generally used with feed-forward neural networks trained with the standard back propagation algorithm. MLPs are supervised networks with feed-forward type, in which each neuron is joined only to the neuron of successive layer and that there are no connections of the feed- back type.

In the present work a multi-layer perceptron with back-propagation neural controller has been developed for the prediction of fatigue crack growth in case of constant amplitude loading with interspersed mixed mode (I and II) overload. The neural network has been written in the C^{++} programming language and all the training tests have been performed on a personal computer. It has got three input parameters and one output parameter. The inputs to the neural network controller are as follows:

Stress intensity factor range = “sifr”; Maximum stress intensity factor = “msif”;

Mode-mixity = “mm”

The output from the neural network is as follows:

Crack growth rate = “cgr”

2.2 Neural controller mechanism for crack growth rate prediction

The neural network used is a nine layer perceptron [13]. The chosen number of layers has been selected empirically to facilitate training. The neurons associated with the input and output layers are three and one respectively. The neurons associated in the seven hidden layers are twelve, twenty four, hundred, thirty five, and eight respectively. The neurons are taken in order to give the neural network a diamond shape (Fig. 1). These numbers of hidden neurons have been found empirically. During training and during validation, the input patterns fed to the neural network comprise the following components:

$y_1^{\{1\}}$ = stress intensity factor range (1a)

$y_2^{\{1\}}$ = maximum stress intensity factor (1b)

$y_3^{\{1\}}$ = mode-mixity (1c)

These input values are distributed to the hidden neurons which generate outputs given by (Haykin, 1999):

$$y_s^{\{lay\}} = f\left(v_s^{\{lay\}}\right) \tag{2}$$

where, $v_s^{\{lay\}} = \sum_r W_{sr}^{\{lay\}}.y_r^{\{lay-1\}}$ (3)

'lay' = layer number (2 to 8)

s = label for s^{th} neuron in the hidden layer 'lay'

r = label for r^{th} neuron in hidden layer 'lay-1'

$W_{sr}^{\{lay\}}$= weight of the connection from neuron r in layer 'lay-1' to neuron s in layer 'lay'

f (.) = activation function, chosen in this work as the hyperbolic tangent function:

$$f(x) = \frac{e^x - e^{-x}}{e^x + e^{-x}} \tag{4}$$

During training, the network output θ_{actual}, may differ from the desired output $\theta_{desired}$ as specified in the training pattern presented to the network. A measure of the performance of the network is the instantaneous sum-squared difference between $\theta_{desired}$ and θ_{actual} for the set of presented training patterns:

$$E_{rr} = \frac{1}{2} \sum_{\substack{all \\ training \\ patterns}} (\theta_{desired} - \theta_{actual})^2 \tag{5}$$

where θ_{actual} represents crack growth rate ("cgr")

The error back-propagation method is employed to obtain the network. This method requires the computation of local error gradients in order to determine appropriate weight corrections to reduce 'E_{rr}'. For the output layer, the error gradient $\delta^{\{9\}}$ is:

$$\delta^{\{9\}} = f'\left(V_1^9\right)(\theta_{desired} - \theta_{actual}) \tag{6}$$

The local gradient for neurons in hidden layer {lay} is given by:

$$\delta_s^{\{lay\}} = f'\left(V_s^{\{lay\}}\right)\left(\sum_k \delta_k^{\{lay+1\}} W_{ks}^{\{lay+1\}}\right) \tag{7}$$

The synaptic weights are updated according to the following expressions:

$$W_{sr}(t+1) = W_{sr}(t) + \Delta W_{sr}(t+1) \tag{8}$$

and $\Delta W_{sr}(t+1) = \alpha \Delta W_{sr}(t) + \eta \delta_s^{\{lay\}} y_r^{\{lay-1\}}$ (9)

where,

α = momentum coefficient (chosen empirically as 0.2 in this work)

η = learning rate (chosen empirically as 0.35 in this work)

t = iteration number, each iteration consisting of the presentation of a training pattern and correction of the weights.

The final output from the neural network is:

$$\theta_{\text{actual}} = \text{f}\left(V_1^{\{9\}}\right) \tag{10}$$

$$\text{where, } V_1^{\{9\}} = \sum_r W_{1\text{r}}^{\{9\}} y_{\text{r}}^{\{8\}} \tag{11}$$

3. Experimental database

The experimental database employed in the present investigation has been taken exclusively from the author's previous work [11]. It consists of six sets of fatigue tests at different overloading angles, β (=0^o, 18^o, 36^o, 54^o, 72^o and 90^o) at overload ratio of 2.5. The interspersed mixed mode (I and II) overload fatigue tests were conducted using 7020 T7 and 2024 T3 Al-alloys with single-edge notched tension specimens on *Instron*-8502 machine. The test specimens were fatigue pre-cracked under mode-I loading to an *a/w* ratio of 0.3 and were subsequently subjected to constant load test (i.e. progressive increase in ΔK with crack extension) maintaining a load ratio of 0.1 at a frequency of 6 Hz. Then the fatigue crack was allowed to grow up to an *a/w* ratio of 0.4 and then subjected to single overload spike at a loading rate of 8 kN/min followed by constant load fatigue test in mode I. For more details about the tests, material properties and loading device the author's previous work [11] can be consulted.

4. Application design and results

4.1 Development of ANN model

While developing an ANN model, proper selection of input and output parameters and also the structure of the network are very much essential in achieving better results. It is considered that the most suitable combinations of input and output sets are those which would give the least normalized mean square error (NMSE). It has now been proved that fatigue crack growth rate is governed not only by single crack driving force ΔK, but,

according to Unified Approach, by the simultaneous action of both ΔK and K_{max} [14-17]. In case of interspersed mixed-mode (I and II) overload, the angle of overloading also influences the retardation effects as verified in various literatures [1, 2, 11]. Therefore, stress intensity factor range (ΔK), maximum stress intensity factor (K_{max}), and mode-mixity $\left(\frac{K_{II}}{K_I + K_{II}}\right)$ have been considered as the best sets of input parameters for the present investigation. As regards the output, crack growth rate $\left(\frac{da}{dN}\right)$ has been chosen as the best output parameter to facilitate prediction of life as well as determination of various retardation parameters.

In order to design a suitable ANN architecture, normalization of input and output parameters are essential. Certain classical normalization, where the range is scaled between 0 and 1, may not be applicable in every ANN model. To make the input amenable for successful learning to minimize the overall mean square error, the two input parameters ΔK and K_{max} have been normalized between 1 and 4, while the other one, mode-mixity $\left(\frac{K_{II}}{K_I + K_{II}}\right)$has been normalized between 0 and 1. Similarly the output $\left(\frac{da}{dN}\right)$ has been normalized between 0 and 3 for network training and testing. The inputs and outputs of the training sets (TS) have been constituted from 3×50 experimental values of ΔK, K_{max} and $\left(\frac{da}{dN}\right)$data for each of the overloading angles 0°, 18°, 36°, 72° and 90° with mode-mixity of 0, 0.245, 0.421, 0.755 and 1.0 in case of both 7020 T7 and 2024 T3 Al-alloys.

4.2 Application of the model

The multi-layer perceptron (MLP) neural network architecture has been applied to simulate the crack growth rate of an unknown set of overload angle, 54^o (mode-mixity = 0.579) as validation set (VS) by constructing a training set (TS) with five known sets of overload angles (β = 0°, 18°, 36°, 72°, 90° and mode-mixity = 0, 0.245, 0.421, 0.755 and 1). The performance of the trained ANN model has been presented in Table 1. Figures 2

and 3 illustrate the mean square error (MSE) curves during the training of the model. After training, the three input parameters i.e. stress intensity factor range (ΔK), maximum stress intensity factor (K_{max}) and mode-mixity (MM) for the suppressed overload angle 54° have been fed to the trained ANN model in order to predict the corresponding crack growth rate $\left(\frac{da}{dN}\right)$. The predicted crack growth rate results of the tested specimens have been presented in Figs. 4 and 5 respectively along with experimental data for comparison. It is observed that the simulated da/dN–ΔK points follow the experimental ones quite well. The number of cycles has been calculated from the simulated $\left(\frac{\mathrm{d}a}{\mathrm{d}N}\right)$ values by taking the experimental *'a'* and *'N'* values of the overload point as the initial values and assuming an incremental crack length of 0.05mm in steps in excel sheet as per following equation:

$$N_{i+1} = \frac{a_{i+1} - a_i}{da/dN} + N_i \tag{12}$$

The predicted $a \sim N$ values of the ANN model have been compared with the experimental data in Figs. 6 and 7 respectively for both the materials. The a–da/dN and N–da/dN curves have been given in Figs. 8 to 11 in order to facilitate the calculation of various retardation parameters (a_d, N_d) as presented in Table-2.

4.3 Comparison with 'exponential model'

The predicted ANN results have been compared quantitatively in Table 2 with that of author's previously proposed "Exponential Model" [11]. For the purpose some silent features of the model need to be discussed here. The fundamental equations of the model were:

$$a_j = a_i e^{m_{ij}(N_j - N_i)} \tag{13}$$

$$m_{ij} = \frac{\ln\left(\frac{a_j}{a_i}\right)}{(N_j - N_i)} \tag{14}$$

where, a_i and a_j = crack length in i^{th} step and j^{th} step in 'mm' respectively,

N_i and N_j = No. of cycles in i^{th} step and j^{th} step respectively,

m_{ij}= specific growth rate in the interval *i-j*,

i = No. of experimental steps,

and $j = i+1$

The exponent *'m'*, called specific growth rate, has been correlated with a parameter *'l'* that depends on various material properties (K_C, E, σ_{ys}) and also two crack driving parameters (ΔK, K_{max}) by the following equation:

$$m = A'l^3 + B'l^2 + C'l + D' \tag{15}$$

where, $l = \left[\left(\frac{\Delta K}{K_C}\right)\left(\frac{K_{max}}{K_C}\right)\left(\frac{\sigma_{ys}}{E}\right)\right]^{\frac{1}{4}}$

and A', B', C', D' are curve-fitting constants.

The model has been applied with a fixed overload ratio (R_{ol} = 2.5) at different overload angles (β = 0°, 18°, 36°, 54°, 72° and 90°). The values of above constants differ since the amount of retardation varies according to the overload angles. Therefore, each constant of different overload angles (except 54° angle) are correlated with mode-mixity, $\left(\frac{K_{II}}{K_I + K_{II}}\right)$, by a 2nd degree polynomial curve fit so as to give the following sets of equations:

$$A' = X_1\left[\frac{K_{II}}{K_I + K_{II}}\right]^2 + Y_1\left[\frac{K_{II}}{K_I + K_{II}}\right] + Z_1 \tag{16}$$

$$B' = X_2\left[\frac{K_{II}}{K_I + K_{II}}\right]^2 + Y_2\left[\frac{K_{II}}{K_I + K_{II}}\right] + Z_2 \tag{17}$$

$$C' = X_3\left[\frac{K_{II}}{K_I + K_{II}}\right]^2 + Y_3\left[\frac{K_{II}}{K_I + K_{II}}\right] + Z_3 \tag{18}$$

$$D' = X_4\left[\frac{K_{II}}{K_I + K_{II}}\right]^2 + Y_4\left[\frac{K_{II}}{K_I + K_{II}}\right] + Z_4 \tag{19}$$

where, X_1…..X_4, Y_1…….Y_4 and Z_1….Z_4 are another set of curve fitting constants relating A', B', C' and D' with mode-mixity $\left(\frac{K_{II}}{K_I + K_{II}}\right)$.

Putting the values of various constants in equation (15) the predicted *'m'* value has been determined for overload angle 54°. The number of cycles (fatigue life) has been calculated case cycle-by-cycle basis as follows;

$$N_j = \frac{\ln\left(\frac{a_j}{a_i}\right)}{m_{ij}} + N_i \qquad (20)$$

The various predicted model results have been presented graphically in Figs. 12 to 19.

5. Analysis of results

The performances of different models were analyzed by comparing the prediction results with the experimental findings by the following criteria:

- Percentage deviation of predicted data from the experimental data i.e. $\%\,\text{Dev} = \frac{\text{Predicted result} - \text{Experimental result}}{\text{Experimental result}} \times 100$
- Prediction ratio which is defined as the ratio of actual result (i.e. experimental) to predicted result i.e.

  Prediction ratio, $P_r = \frac{\text{Actual result}}{\text{Predicted result}}$
- Error bands i.e. the scatter of the predicted life in either side of the experimental life within certain error limits.

Table 3 presents various model results as per the above evaluation criteria. From the above table it is observed that the percentage deviations of different retardation parameters are within $\pm 7.0\%$ (maximum). The post overload fatigue crack propagation lives are within –0.2% to +1.5% whereas, the prediction ratio is about 1.0. From the above results it can be concluded that the performance of ANN model is quite satisfactorily. As far as relative performance is concerned, the exponential model gives better results in comparison to ANN model. Analyzing the error band scatter (Figs. 20 and 21) it is observed that the results of Al 7020 T7 are within $\pm 0.05\%$ error band while, it is less i.e. $\pm 0.025\%$ for Al 2024 T3.

6. Discussion and Conclusion

Prediction of residual fatigue life including the retardation parameters (a_d and N_d) under interspersed mixed-mode (I and II) overloads by the proposed ANN model provided an excellent matching with the experimental data and also with the exponential model proposed earlier by the authors. It is observed that the ANN result is seriously affected by the selection of input and output parameters. Selecting single crack driving force (ΔK), instead of two crack driving forces (ΔK and K_{max}) and mode-mixity (MM) as inputs, resulted in poor prediction of crack growth rate (da/dN). This supports the principle of Unified Approach which has been taken into consideration in formulating the Exponential Model. Inclusion of the suppressed data set for overload angle 54° (which has been predicted from the model) may further improve the accuracy of the ANN model, which can be used to predict any intermediate angle within the range 0° to 90°. However, one of the shortcomings of the present ANN model is that the life is calculated from the predicted crack growth rate results, whereas the direct prediction of fatigue life is possible in case of "Exponential Model".

Acknowledgement

The authors wish to record their thanks to CSIR, India for sponsoring this project (project No. 22(373)/04/EMR II). They also thank Hindalco, Renukoot (UP), India for supplying the Aluminium alloy for this research project.

References

1. Srinivas V, Vasudevan P (1993). Studies of mixed-mode crack propagation in D16AT Al-alloy. *Eng. Fract. Mech.*, **45**(4), 415-30.
2. Sander M, Richard HA (2006). Experimental and numerical investigations on the influence of the loading direction on the fatigue crack growth. *Int. J. Fatigue*, **28**, 583-91.
3. Iida S, Kobasahi AS (1969). Crack propagation in 7075-T6 plates under cyclic tensile and transverse shear loadings. *J Bas. Eng. Series*, **D91**, 764-69.
4. Patel AB, Pandey RK (1981). Fatigue crack growth under mixed-mode loading. *Fatigue Fract. Engng. Mater. Structures*, **6**, 65-77.

5. Socie DF (1977). Prediction of Fatigue Crack Growth in Notched Members under Variable Amplitude Loading Histories. *Eng. Fract. Mech.*, **9** ,849–65.

6. Chen WR, Keer LM (1991). Fatigue Crack Growth in Mixed-Mode Loading. *J. Eng. Mater. Tech.*, **113**(2), 222–27.

7. Tamilselvan T, Lo KW, Gong YB, Zhao MM (2005). A Model for Mixed-Mode Fatigue. *J Testing Evalution*, **33**(3), 188-96.

8. Kim JK, Kim CS (2002). Fatigue crack growth behavior of rail steel under mode-I and mixed mode loadings. *Mater. Sc. Eng.*, **A338**, 191-201.

9. Sander M, Richard HA (2005). Finite element analysis of fatigue crack growth with interspersed mode I and mixed mode overloads. *Int. J. Fatigue*, **27**, 905-13.

10. Mohanty JR, Verma BB, Ray PK (2008). Evaluation of Overload-induced Fatigue Crack Growth Retardation Parameters using an Exponential Model. *Eng. Fract. Mech.*, **75**, 3941-51.

11. Mohanty JR, Verma BB, Ray PK (2009). Prediction of fatigue life with interspersed mode-I and mixed mode (I and II) overloads by an Exponential Model: Extensions and improvements. *Eng. Fract. Mech.*, doi:10.1016/j.engfracmech.2008.12.001.

12. Jia J, Davalos JF (2006). An artificial neural network for the fatigue study of bonded FRP-wood interfaces. *Comp. Struct.*, **74**(1), 106-14.

13. Haykin S (1999). *Neural networks: a comprehensive foundation*. Macmillan, New York.

14. Donald K, Paris PC (1999). An evaluation of ΔK_{eff} estimation procedures on 6060-T6 and 2024-T3 aluminum alloys. *Int. J. Fatigue*, **21**(suppl.1), S47-57.

15. Dinda S, Kujawski D (2004). Correlation and prediction of fatigue crack growth for different R-ratios using K_{max} and ΔK^{+} parameters. Eng. Fract. Mech., **71**(12), 1779-90.

16. Kujawski D (2001). A new $(\Delta K^{+} K_{max})^{0.5}$ driving force parameter for crack growth in aluminum alloys. *Int. J. Fatigue*, **23**(8), 733-40.

17. Noroozi AH, Glinka G, Lambert S (2005). A two parameter driving force for fatigue crack growth analysis. *Int. J. Fatigue*, **27**(10-12), 1277-96.

List of Tables

1. Performance of ANN model during training

2. Comparison of ANN and exponential model results with experimental data

3 – Percentage deviations retardation Parameters under mixed mode overload

List of Figures

1. ANN architecture

2. MSE curve obtained during training of ANN for Al 7020 T7

3. MSE curve obtained during training of ANN for Al 2024 T3

4. Comparison of predicted (ANN) and experimental crack growth rate with stress intensity factor range for overload angle of 54^o(Al 7020 T7)

5. Comparison of predicted (ANN) and experimental crack growth rate with stress intensity factor range for overload angle of 54^o (Al 2024 T3)

6. Comparison of predicted ANN result (54^o) of crack length with number of cycles (Al 7020 T7)

7. Comparison of predicted ANN result (54^o) of crack length with number of cycles (Al 2024 T3)

8. Comparison of predicted ANN result (54^o) of crack growth rate with crack length (Al 7020 T7)

9. Comparison of predicted ANN result (54^o) of crack growth rate with crack length (Al 2024 T3)

10. Comparison of predicted ANN result (54^o) of crack growth rate with number of cycles (Al 7020 T7)

11. Comparison of predicted ANN result (54^o) of crack growth rate with number of cycles (Al 2024 T3)

12. Comparison of predicted (ANN), 'Exponential Model' and experimental results (54^o) of crack length with number of cycles (Al 7020 T7)

13. Comparison of predicted (ANN), 'Exponential Model' and experimental results (54^o) of crack length with number of cycles (Al 2024 T3)

14. Comparison of predicted ANN and 'Exponential Model' results (54^o) values of crack growth rate with stress intensity factor range (Al 7020 T7)

15. Comparison of predicted ANN and 'Exponential Model' results (54^o) of crack growth rate with stress intensity factor range (Al 2024 T3)
16. Comparison of predicted (ANN), Exponential and experimental crack growth rate with crack length for 54^o (Al 7020 T7)
17. Comparison of predicted (ANN), Exponential and experimental crack growth rate with crack length for 54^o (Al 2024 T3)
18. Comparison of predicted (ANN), Exponential and experimental crack growth rate with number of cycle for 54^o (Al 7020 T7)
19. Comparison of predicted (ANN), Exponential and experimental crack growth rate with number of cycle for 54^o (Al 2024 T3)
20 – Error band scatter of predicted lives of 7020 T7 under mixed mode overload
21 – Error band scatter of predicted lives of 2024 T3 under mixed mode overload

Table 1 – Performance of ANN model during training

Material	Momentum Coefficient	Learning rate	Hidden neurons	MSE	Training epochs	Computational Time (Min.)
7020 T7	0.2	0.35	179	1.688×10^{-6}	7.419×10^{5}	765
2024 T3	0.2	0.35	179	1.798×10^{-6}	7.789×10^{5}	686

Table 2 – Comparison of ANN and exponential model results with experimental data

Test sample	a_d^A mm	a_d^{EN} mm	a_d^{EX} mm	N_d^A *K cy.*	N_d^{EN} *K cy.*	N_d^{EX} *K cy.*	N_f^A *K cy.*	N_f^{EN} *K cy.*	N_f^{EX} *K cy.*
7020-T7	1.900	1.978	1.994	22.547	21.49	21.750	75.493	74.60	74.778
2024-T3	2.141	2.274	2.300	20.791	19.564	20.019	120.152	118.22	118.475

Table 3 – Various model results under interspersed mode-I overload

Test sample	% Dev a_d^{EN}	% Dev $a_{\mathrm{d}}^{\mathrm{A}}$	% Dev N_d^{EN}	% Dev $N_{\mathrm{d}}^{\mathrm{A}}$	% Dev (N_f^{EN})	% Dev ($N_{\mathrm{f}}^{\mathrm{A}}$)	Prediction ratio of exponential model (P_r^{EN})	Prediction ratio of ANN (P_r^A)
7020 T7	–0.80	–4.71	–1.20	+3.66	–0.241	+0.956	1.0024	0.991
2024 T3	–1.13	–6.91	–2.27	+3.86	–0.219	+1.415	1.0021	0.986

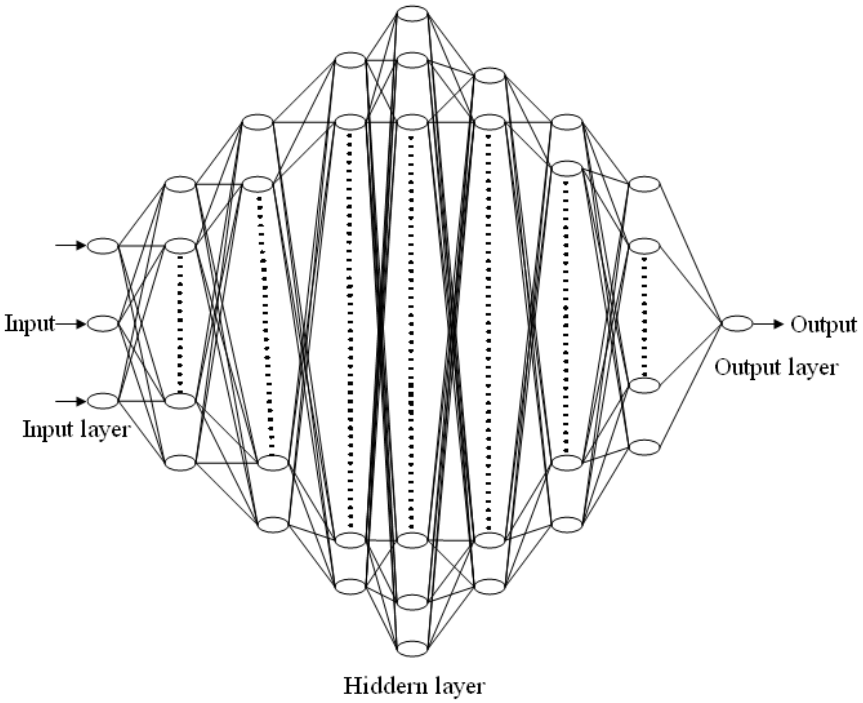

Fig. 1 - ANN architecture

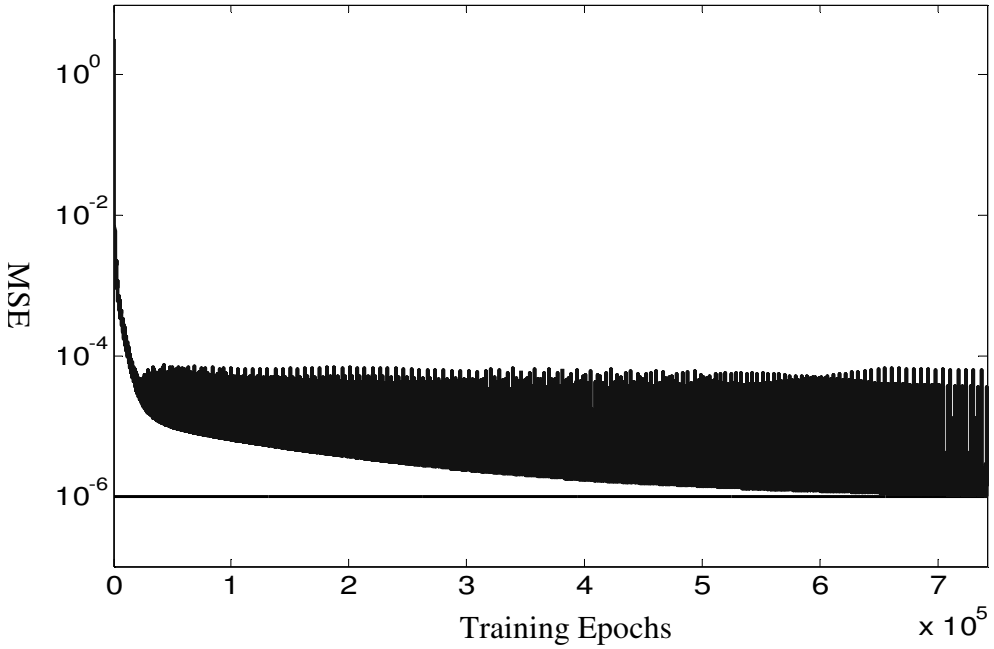

Fig. 2 – MSE curve obtained during training of ANN for Al 7020 T7

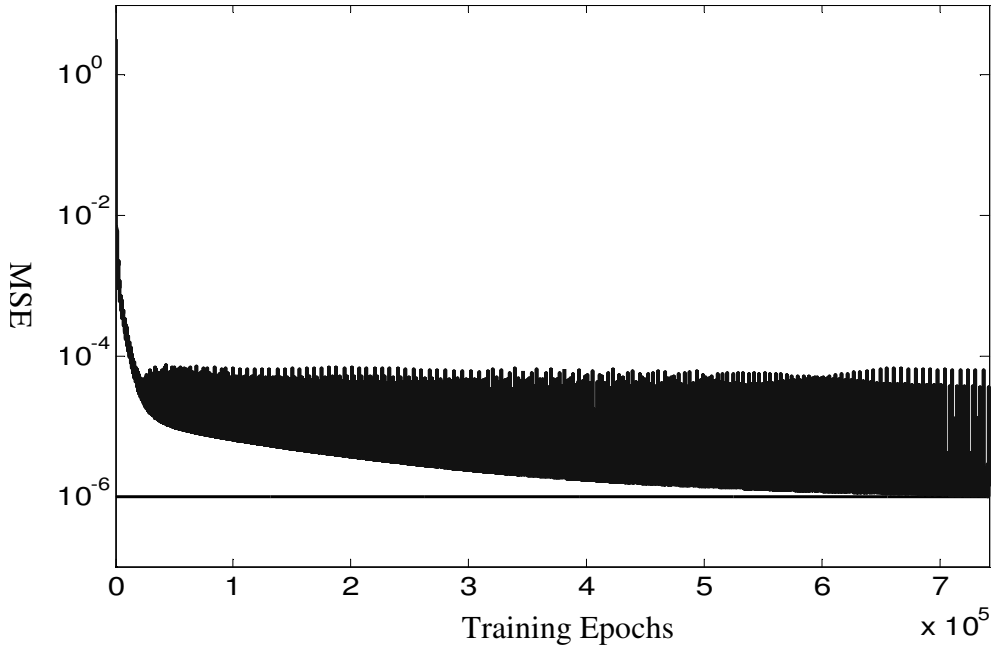

Fig. 3 – MSE curve obtained during training of ANN
for Al 2024 T3

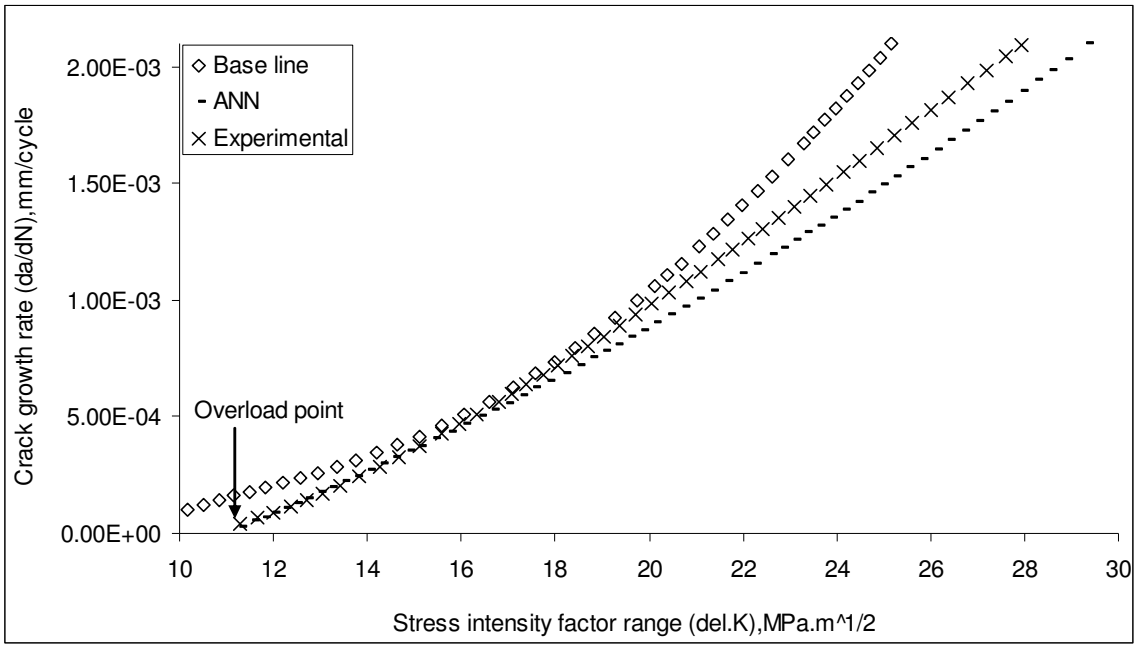

Fig. 4 - Comparison of predicted (ANN) and experimental crack growth rate
with stress intensity factor range for overload angle of 54^{o}(Al 7020 T7)

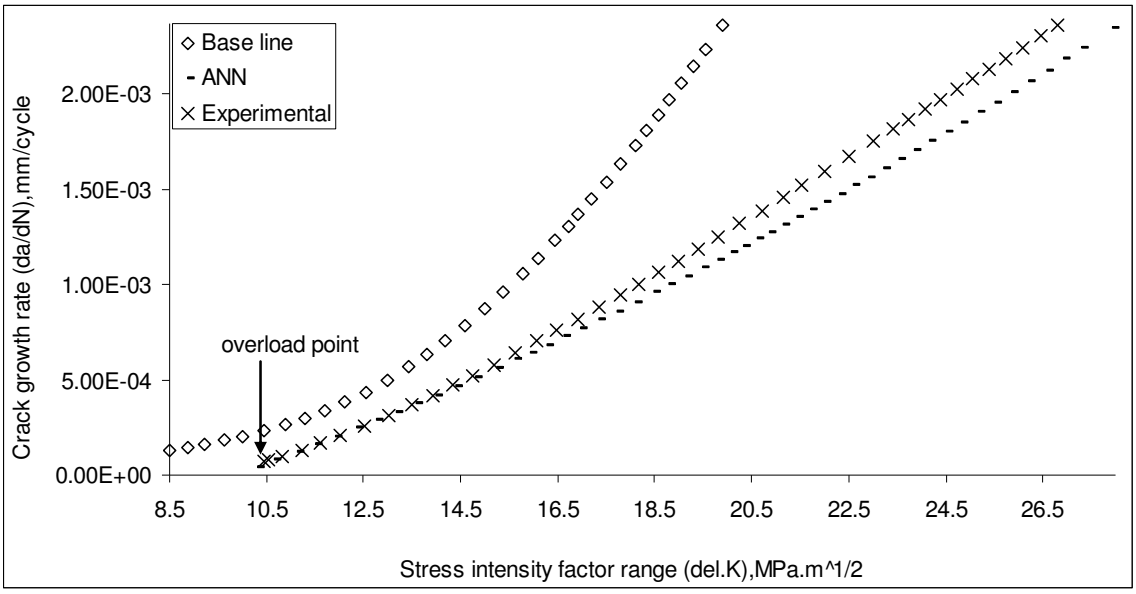

Fig. 5 - Comparison of predicted (ANN) and experimental crack growth rate with stress intensity factor range for overload angle of 54^{o} (Al 2024 T3)

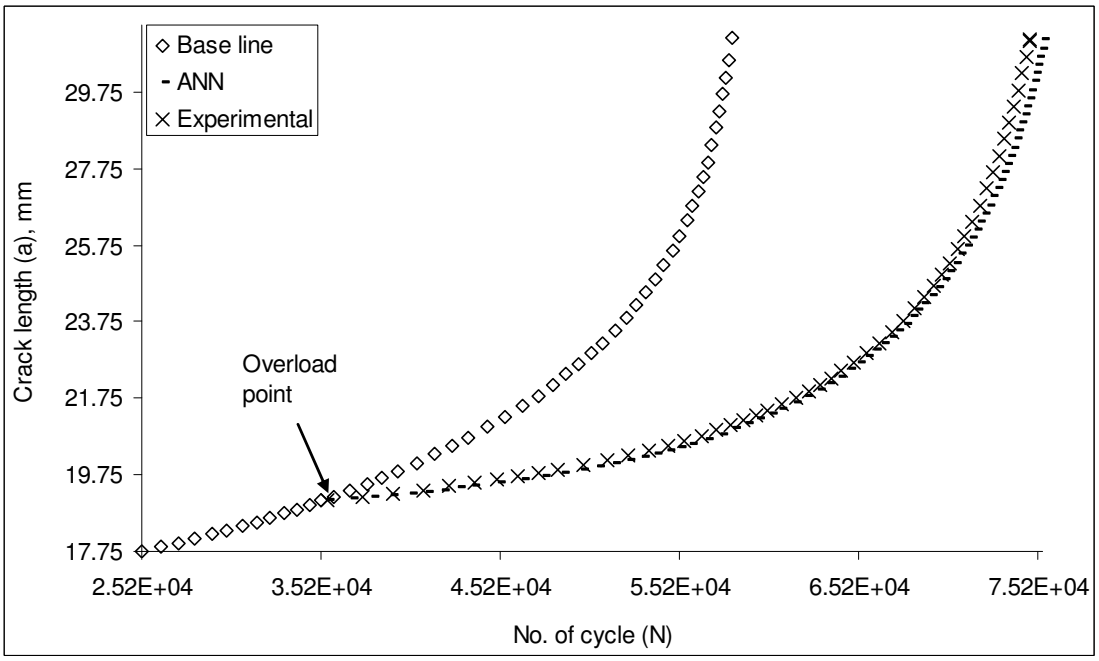

Fig. 6 - Comparison of predicted ANN result (54^{o}) of crack length with number of cycles (Al 7020 T7)

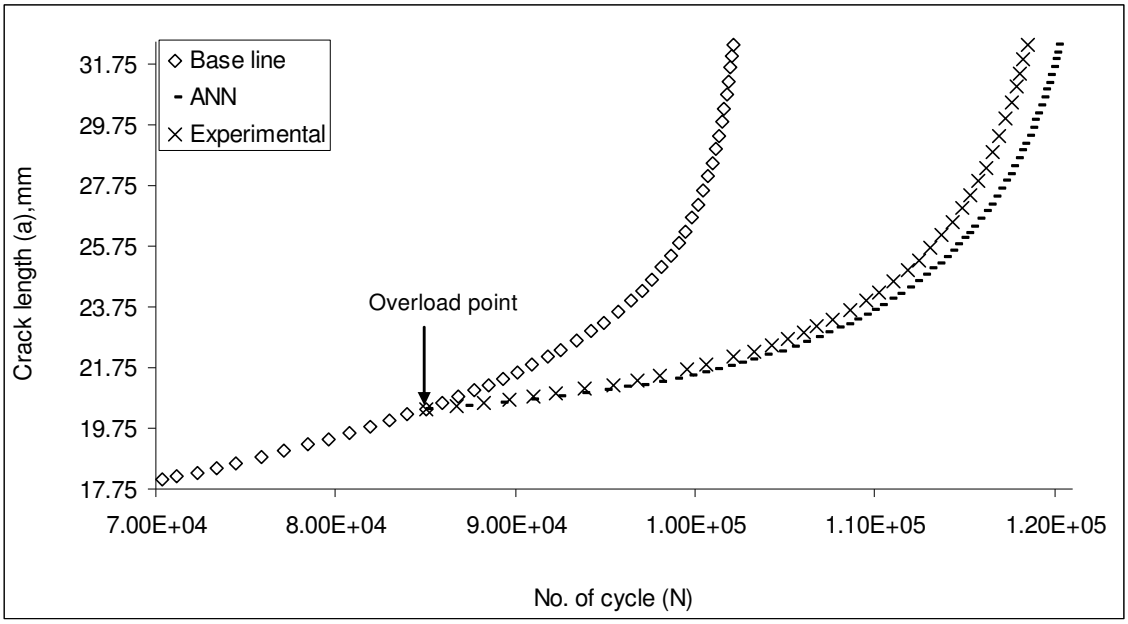

Fig. 7 - Comparison of predicted ANN result (54^{o}) of crack length with number of cycles (Al 2024 T3)

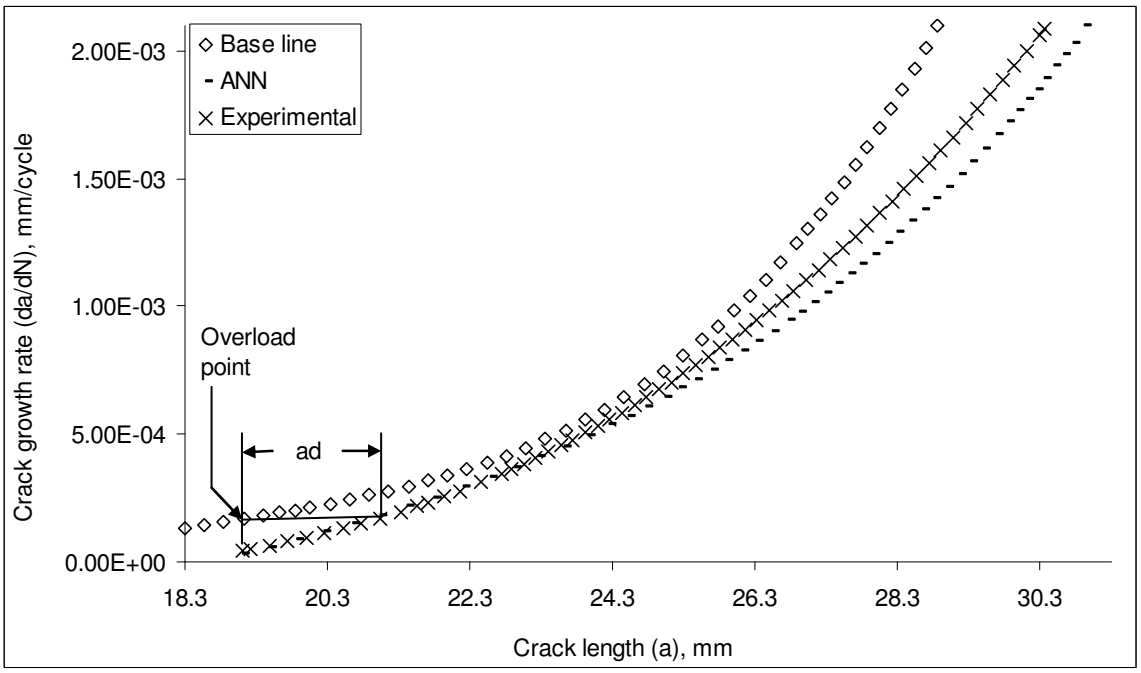

Fig. 8 - Comparison of predicted ANN result (54^{o}) of crack growth rate with crack length (Al 7020 T7)

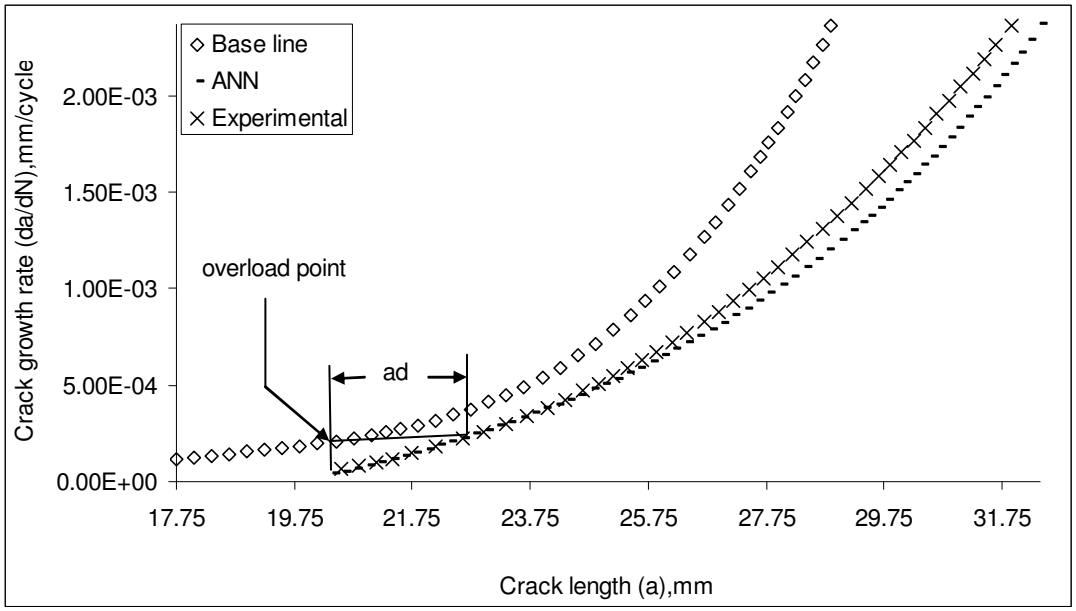

Fig. 9 - Comparison of predicted ANN result (54^{o}) of crack growth rate with crack length (Al 2024 T3)

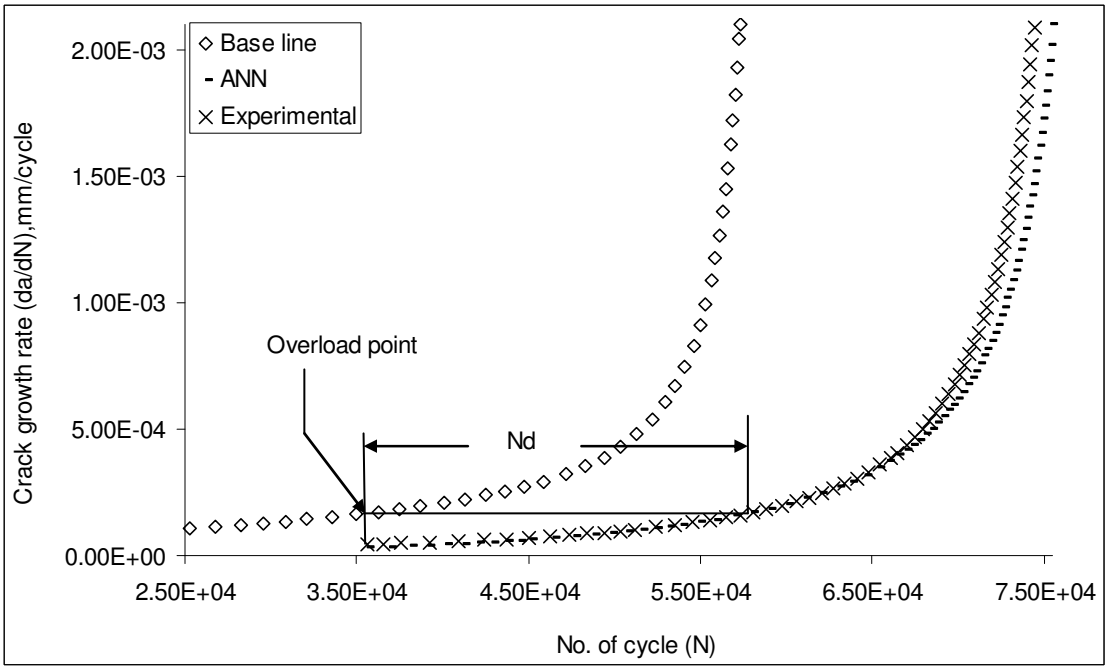

Fig. 10 - Comparison of predicted ANN result (54^{o}) of crack growth rate with number of cycles (Al 7020 T7)

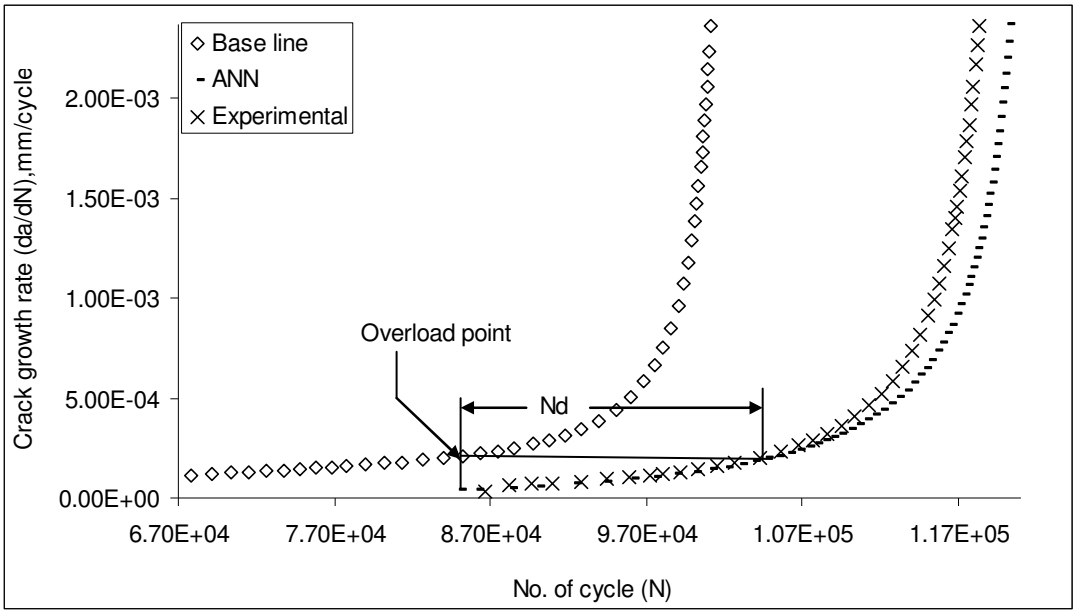

Fig. 11 - Comparison of predicted ANN result (54^{o}) of crack growth rate with number of cycles (Al 2024 T3)

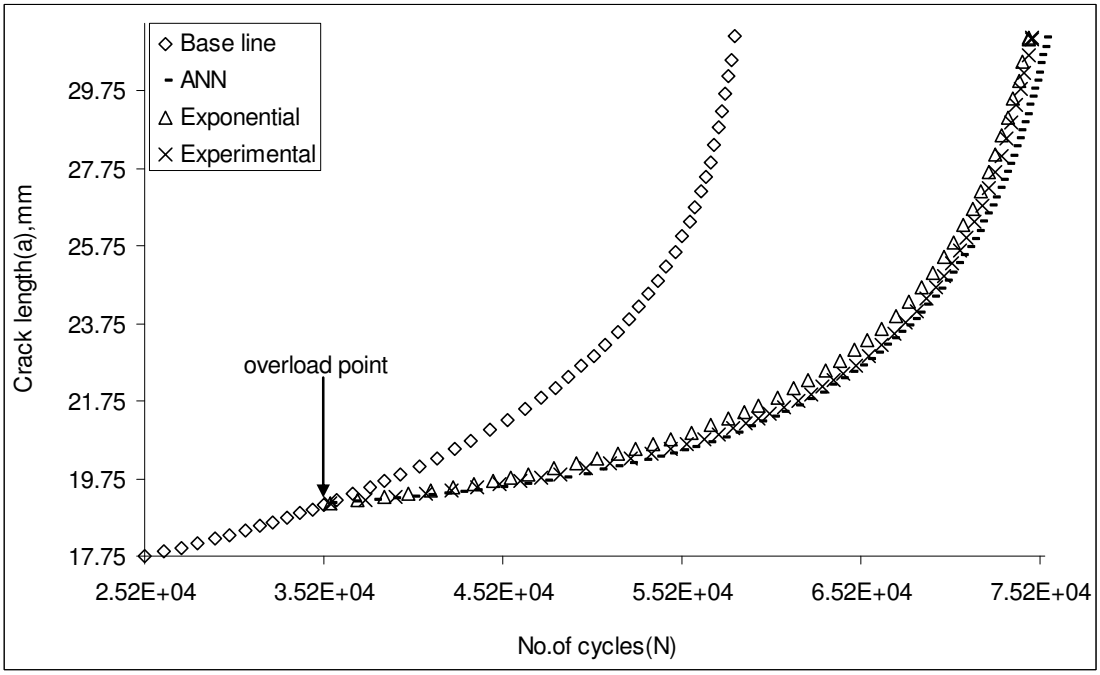

Fig. 12 - Comparison of predicted (ANN), 'Exponential Model' and experimental results (54^{o}) of crack length with number of cycles (Al 7020 T7)

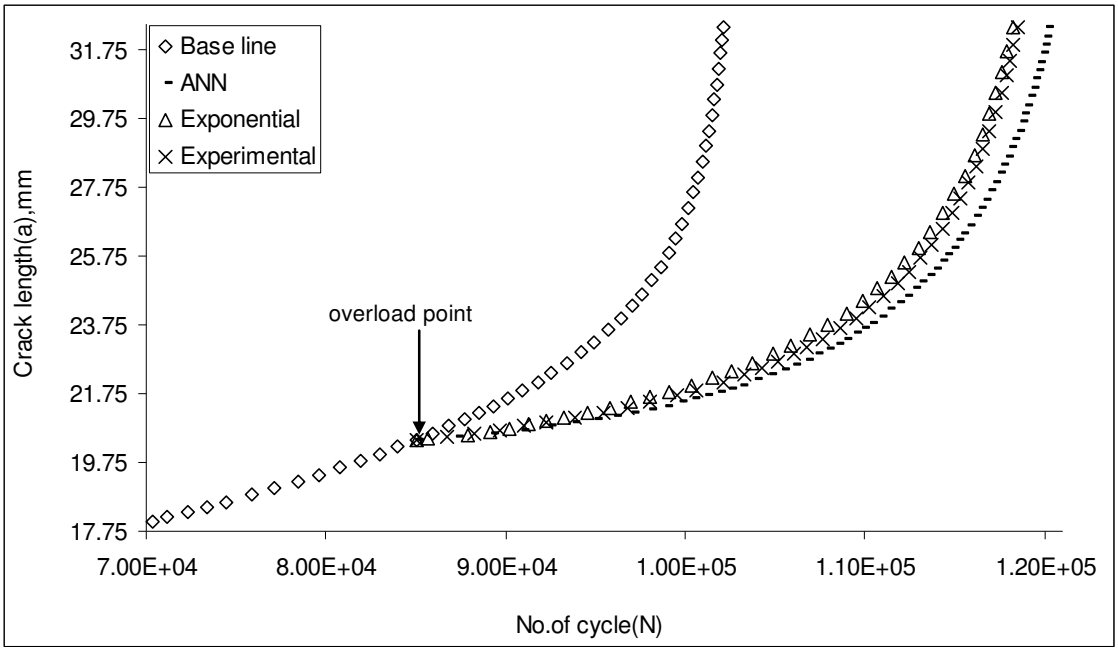

Fig. 13 - Comparison of predicted (ANN), 'Exponential Model' and experimental results (54^{o}) of crack length with number of cycles (Al 2024 T3)

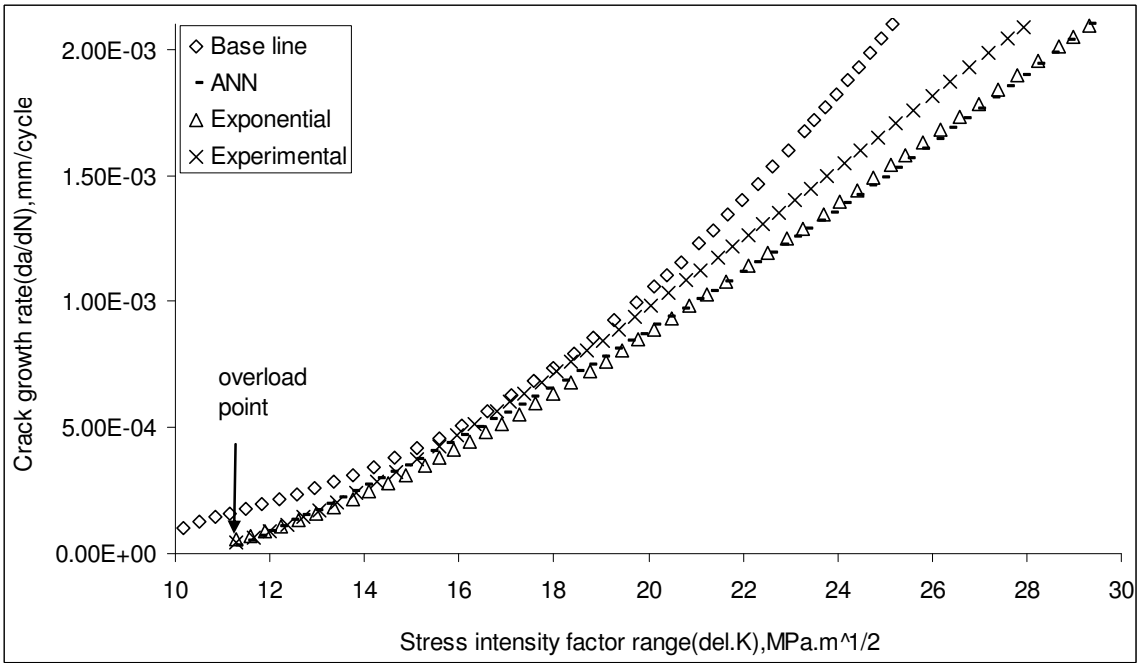

Fig. 14 - Comparison of predicted ANN and 'Exponential Model' results (54^{o}) of crack growth rate with stress intensity factor range (Al 7020 T7)

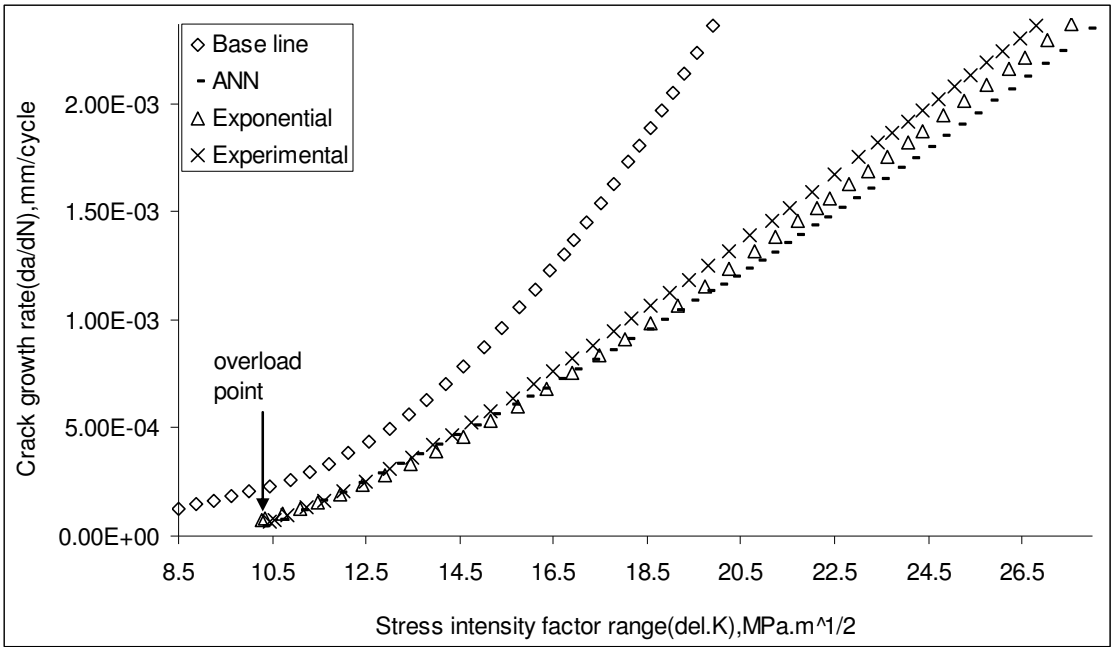

Fig. 15 - Comparison of predicted ANN and 'Exponential Model' results (54^{o}) of crack growth rate with stress intensity factor range (Al 2024 T3)

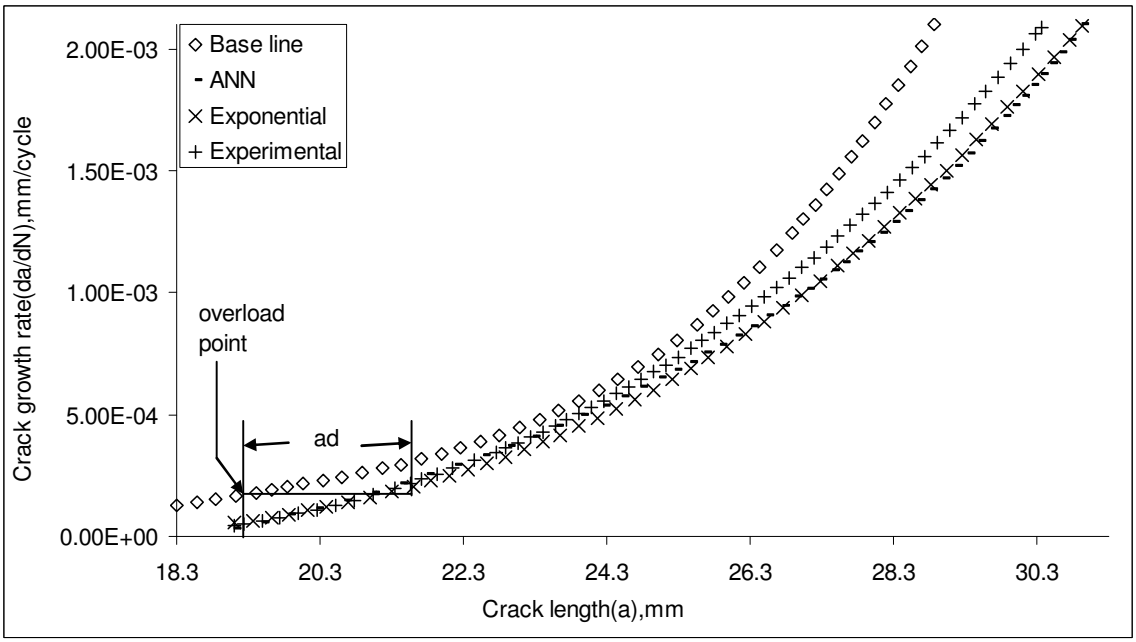

Fig. 16 - Comparison of predicted (ANN), Exponential and experimental crack growth rate with crack length for 54^{o} (Al 7020 T7)

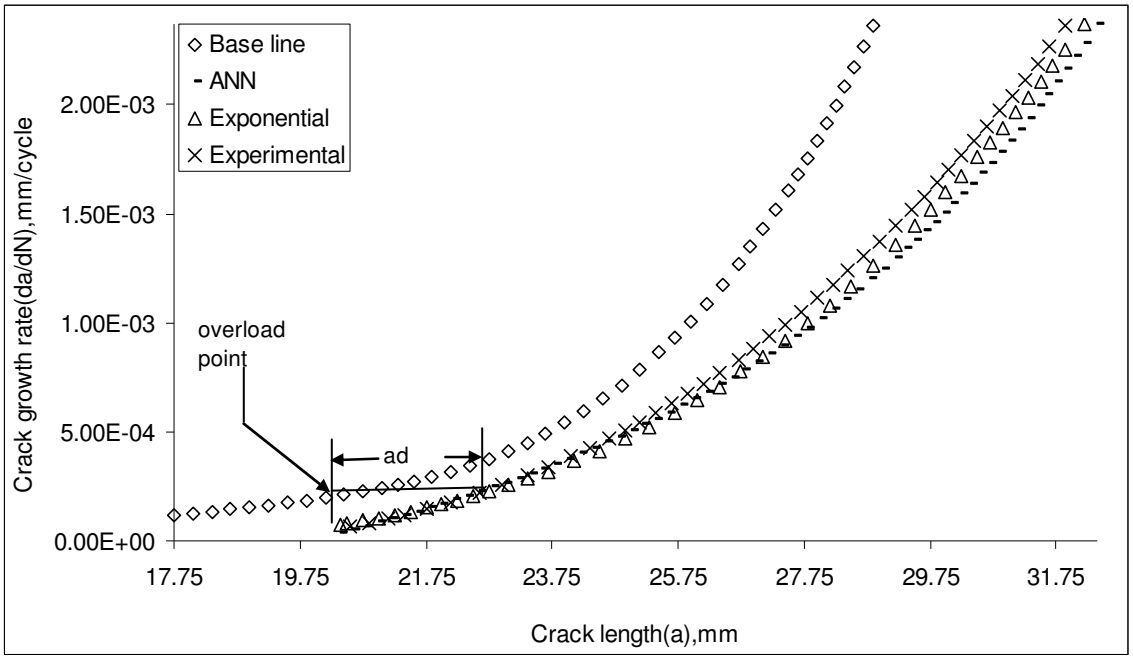

Fig. 17 - Comparison of predicted (ANN), Exponential and experimental crack growth rate with crack length for 54^{o} (Al 2024 T3)

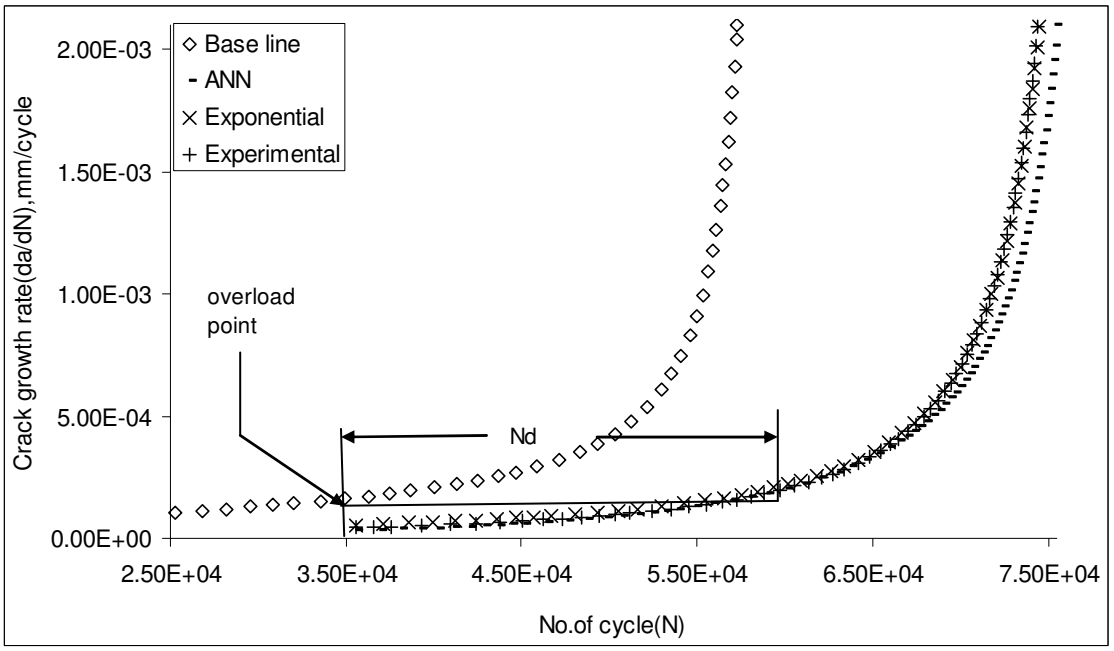

Fig. 18 - Comparison of predicted (ANN), Exponential and experimental crack growth rate with number of cycle for 54^{o} (Al 7020 T7)

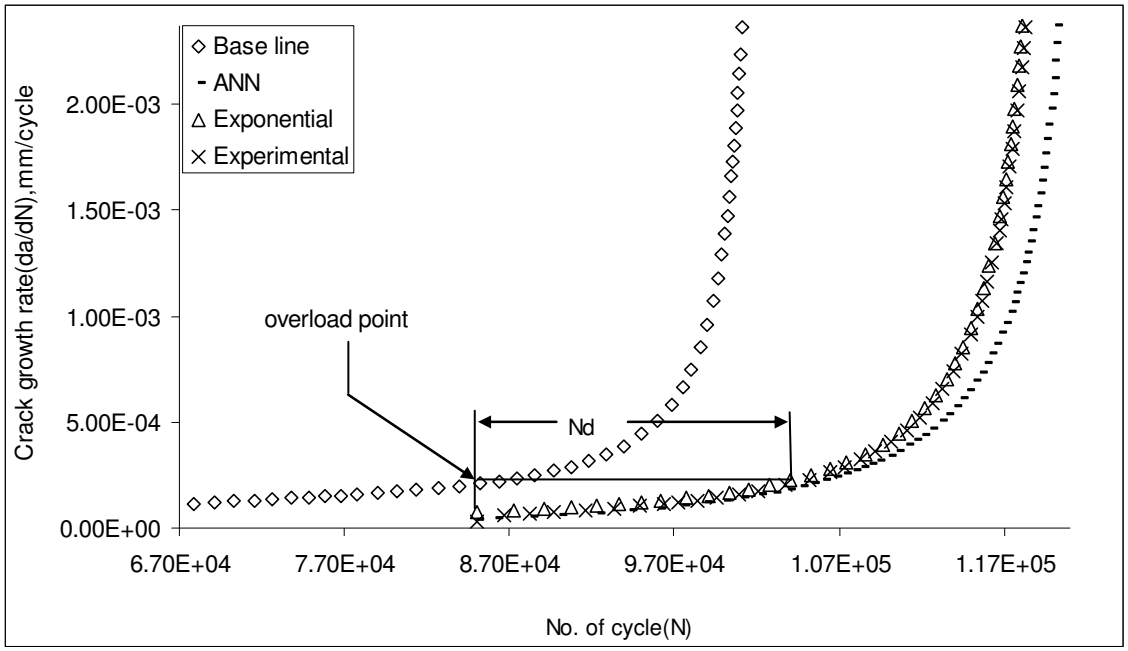

Fig. 19 - Comparison of predicted (ANN), Exponential and experimental crack growth rate with number of cycle for 54^{o} (Al 2024 T3)

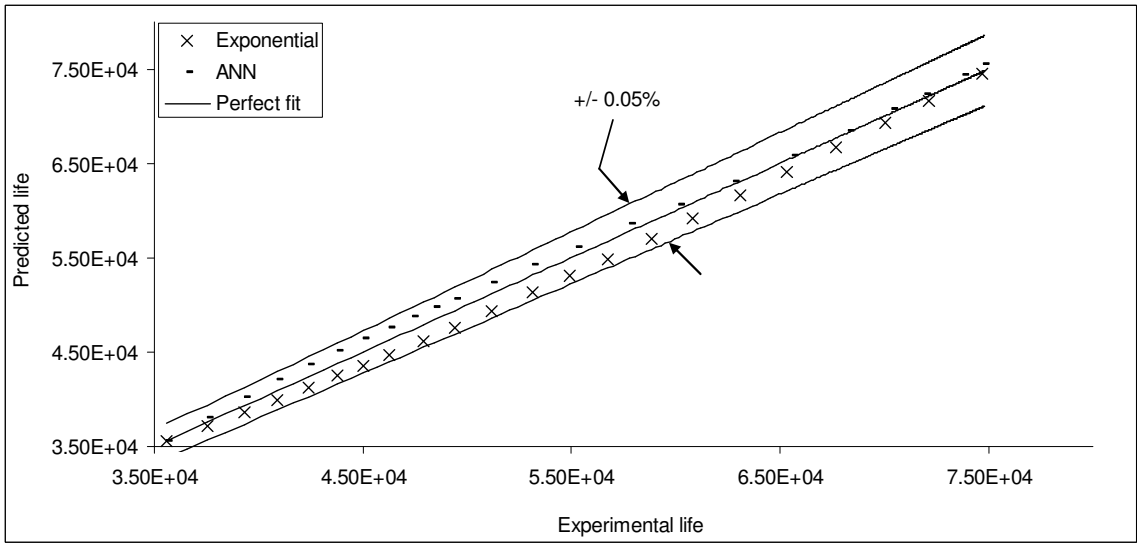

Fig. 20 – Error band scatter of predicted lives of 7020 T7 under mixed mode overload

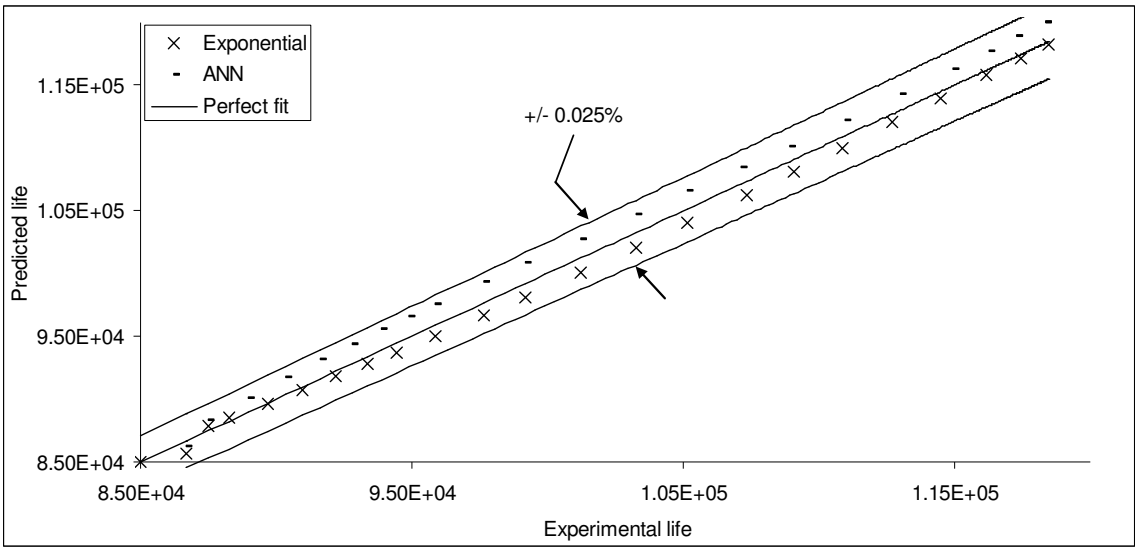

Fig. 21 – Error band scatter of predicted lives of 2024 T3 under mixed mode overload